Frazil Deposition Under Growing Sea Ice

M.J. McGuinness,[1,4] M.J.M. Williams,[2] P.J. Langhorne,[3] C. Purdie,[3] J. Crook[4]

Abstract. Platelet ice may be an important component of Antarctic land-fast sea ice. Typically, it is found at depth in first-year landfast sea ice cover, near ice shelves. To explain why platelet ice is not commonly observed at shallower depths, we consider a new mechanism. Our hypothesis is that platelet ice eventually appears due to the sudden deposition of frazil ice against the fast ice-ocean interface, providing randomly oriented nucleation sites for crystal growth. Brine rejected in plumes from land-fast ice generates stirring sufficient to prevent frazil ice from attaching to the interface, forcing some of it to remain in suspension until ice growth rate and brine rejection slow to the point that frazil can stick. We calculate a brine plume velocity, and match this to frazil rise velocity. We consider both laminar and turbulent environments. We find that brine plume velocities are generally powerful enough to prevent a significant range of frazil sizes from sticking in the case of laminar flow, and that in the turbulent case there may be a critical ice thickness at which most remaining circulating frazil suddenly settles.

Accepted for publication in the Journal of Geophysical Research,

1. Introduction

During the early freezing of the ocean, small discs of ice (frazil) accumulate near the surface and eventually stick together to form a relatively solid layer of small randomly oriented crystals, usually about 10cm thick. Then further growth favours crystals with their fastest growth plane near vertical. Columnar ice results, with large crystals and nearly horizontal c-axes (e. g. Eicken, 2003; Weeks and Ackley, 1986).

Another type of ice is commonly observed in Antarctic land-fast sea ice, especially near ice shelves. This is platelet ice, consisting of various-sized, flat, plate-like crystals with disordered c-axis orientations. Platelets have been defined as dendritic single crystals with no inclusions (Moretskii, 1965; Jeffries et al., 1993). They grow up to 200 mm in diameter, and are up to about 3 mm thick. They have also been called frazil ice, but there is a variety of terminology (see Smith, 2001, for a full discussion). They are found both freely circulating as individual crystals in supercooled seawater beneath a solid sea ice cover, and incorporated into the structure of land-fast sea ice. In this paper, we use the term frazil to refer to small ice crystals that drift in the water columns and display as crystals up to about 5 mm in radius when found in a sea ice core, without any implications for genesis. We use the term platelet to refer to crystals that originate in the water column and have a genesis associated with interaction with an ice shelf. Platelets may become attached to and possibly incorporated into the sea ice cover, and there is no implication that platelets are small. There is also no suggestion that frazil cannot grow into platelets, in a supercooled water column or while attached to the sea ice cover.

In the McMurdo Sound region of the Ross Sea, platelet ice is typically observed in fast ice cores at depths greater than about 1 m (Jones and Hill, 2001; Gow *et al*, 1998; Smith *et al*, 1999; Smith *et al*, 2001; Jeffries *et al*, 1993; Leonard *et al*, 2006). In such regions, turbulent tidal ocean flows, episodically supercooled from early winter onwards and carrying billows of frazil ice, complicate the picture (Leonard *et al*, 2006; Jenkins and Bombosch, 1995; Purdie *et al*, 2006). Platelet ice incorporated into fast ice correlates strongly with the presence of frazil in the underlying water column (Leonard *et al*, 2006).

A number of hypotheses have been proposed to explain why platelet ice is commonly found in sea ice cores near ice shelves in Antarctica at ice depths greater than about 1 m, but is largely absent at shallower depths. The presence of ice shelves nearby is known to be important (Crocker and Wadhams, 1989; Holland and Jenkins, 1999; Jenkins and Bombosch, 1995; MacAyeal, 1984), with supercooled plumes leaving the ice shelf at neutral buoyancy levels and moving out under nearby sea ice. Frazil ice in these plumes grows, collides and provides secondary nucleation sites, and rises out of suspension due to buoyancy (Daly, 1984). Rise velocities depend on the volume of the disc-shaped frazil crystals (Gosink and Osterkamp, 1983), as well as disc orientation and turbulence (this work). The platelet ice found in land-fast sea ice may be the result of frazil that has grown entirely in the supercooled plume before rising out of suspension to attach to the fast ice; or it may have grown entirely at the fast ice interface; or a combination of these two mechanisms may occur (Veazey, 1994; Veazey *et al*, 1994; Gow *et al*, 1998; Smith *et al*, 1999; Smith *et al*, 2001). The random orientation of platelets observed in land-fast ice suggests they grow mostly in place (Gow *et al*, 1998), rather than arriving as full-sized crystals, since a large disc would be expected to settle against the fast ice interface with its c-axis almost vertical. However, this argument assumes that the ice-ocean interface is flat compared with the disc size, and that a disc arrives at the interface alone. The delayed appearance of platelets in fast ice in some areas may be due to

[1]Department of Mathematical Sciences, Korea Advanced Institute of Science and Technology, Taejon, South Korea

[2] National Institute of Water and Atmospheric Research, Wellington, New Zealand

[3]Physics Department, University of Otago, Dunedin, New Zealand

[4]currently: School of Mathematics, Statistics and Operations Research, Victoria University of Wellington, New Zealand

0148-0227/09/$9.00

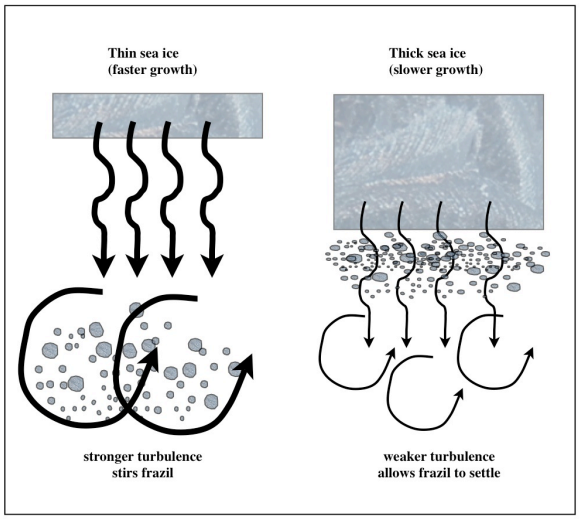

Figure 1. A conceptual sketch illustrating stronger brine-driven turbulence under thinner sea ice, mobilizing frazil ice in the ocean.

the residence time of frazil ice in the supercooled plume; or it may be due to the time required to remove sensible heat from the ocean immediately below the fast ice (Crocker and Wadhams, 1989); or it may be due to the new hypothesis to be outlined here.

The transition that is sometimes seen in Antarctic sea ice, from columnar to platelet ice, has a compelling parallel in the columnar-to-equiaxed crystal transition seen in binary alloy solidification (Badillo and Beckermann, 2006; Ghosh, 2001). Often, with cooling from the outside of a casting of a binary alloy, columnar crystals grow horizontally from the walls towards the centre of the casting as it sets, and small crystals grow in the convecting melt where it has not yet solidified. In the solid casting, a transition from columnar to equiaxed crystals (randomly oriented like our platelets) is seen, associated with the location of the convection front when it sets. Convection of the melt containing growing crystals occurs in the initial stages, and randomises the crystal orientations. Eventually the viscosity of the convecting melt increases and convection ceases, freezing the randomised crystals in place.

There is a key difference between these two applications of solidification of a binary melt — in alloy solidification, the process continues until all of the melt has frozen, and the transition to platelet or equiaxed crystals is associated with the mushy zone taking over the melt region. In the case of sea ice, there is plenty of melt remaining below fast ice at the end of winter; on the other hand, buoyancy effects act to bring frazil crystals up against the fast ice, while turbulence acts to keep them in suspension (Svensson and Omstedt, 1998). It is clear that in the case of alloy solidification, the equiaxed crystals must eventually become part of the solid. It is not so clear in the case of sea ice if and when this transition occurs, and why it should be sudden.

In this paper we consider the role played by brine rejection from growing fast ice, and how it might interact with frazil in the water column. Narrow plumes of cold brine flow down from growing fast ice into the ocean, and slower warmer wider regions of seawater flow up into the permeable lower levels of the fast ice in return. These brine plumes, if they flow rapidly enough, may keep frazil in suspension, so that fast ice is composed of congelation ice. We investigate the possibility that, as the sea ice thickens, the flow in brine plumes may weaken sufficiently that frazil can settle against the fast ice, and become incorporated into it. The situation is summarised in the conceptual sketch in Fig. (1).

The spacing between brine plumes will be less than or equal to the spacing between the small brine tubes seen in cores taken from sea ice (Lake and Lewis, 1970), since each such tube will eject brine in a plume. There may be additional plumes originating, for example, at the tips of dendrites. The small brine tubes have diameters of about 0.4 mm, are spaced about 1.5 mm apart, and occupy about 5% of the surface area of the sea ice.

Frazil and platelet disc sizes are variously reported in the literature. Holland and Feltham (2005) describe frazil discs as having radii in the range 0.01–10 mm. Martin (1981) in his review of field observations of river frazil notes a maximum radius of 0.1–2.5 mm. Laboratory observations indicate radii up to 10 mm (Smedsrud, 2001), and Dieckmann *et al* (1986) trawled platelets with an average radius of 10 mm in a net with a mesh size of 10 mm. Modelling work by Bombosch (1998) also supports disc radii up to 10 mm.

Daly's (1984) theory has a distribution of frazil sizes that falls off very rapidly for radii greater than 1 mm. Other modellers use radii ranging from 0.003 to 5 mm (Jenkins and Bombosch, 1995; Martin, 1981; Svensson and Omstedt, 1994). Aspect ratio (disc thickness over diameter) is typically $\epsilon \approx 0.01$, but may be as large as 0.1. The size spectrum of figure 9 in Smedsrud and Jenkins (2004) arises out of their modelling, and has a peak between 1-2 mm in size, with a range up to 3 mm. The largest disc size in the modelling described by Svensson and Omsted (1998) is 10mm, and while the numbers of such discs may be as high as 10^5 per m^3 at 1m depth, this is a factor of 10^6 smaller than the peak disc numbers at about 0.01mm radius.

These wide ranges and variations in size distributions do not directly affect our calculations, as we make no specific assumptions about frazil sizes under sea ice in these calculations. We do assume for the purposes of our conclusions, that relatively few discs are larger than 5–10 mm in radius, and that most discs are smaller than 3 mm in radius. There is strong support in the above literature for these assumptions.

If the frazil is of a similar length-scale to the roughness of the mushy zone/sea water interface, or if the amount of frazil (previously well-stirred by turbulence) that can settle against the interface is thick enough, then an episodic re-seeding of the fast ice interface with frazil ice with random c-axis orientations and crystal sizes may be associated with times of low turbulence, due to low tidal shear flow. Tidal records from McMurdo Sound, Antarctica (Goring and Pyne, 2003) suggest a 14-day period, associated with the spring/neap tidal cycle. Times of low shear are anticipated due to both this cycle, and to the diurnal tidal cycle.

Subsequent fast-ice growth during more vigorous shear flow will be from these newly adhered randomly oriented seed crystals, and might be expected to have the characteristics of platelet ice, with sizes limited by the time until the next low shear episode allows new seeds to settle, and also limited by the geometric exclusion of crystals with more vertically oriented c-axes that eventually (in the absence of re-seeding) leads to columnar ice with horizontal c-axes.

In the following sections, we use solid sea ice growth rates measured in the field, to calculate brine plume velocities as a function of sea ice thickness. Frazil rise velocities in still and turbulent water are used to calculate the plume velocity that will mobilise frazil ice of a given radius, leading to a relationship between fast ice thickness and the maximum size of frazil that is kept in suspension. In the case of a turbulent ocean, we find there is a sudden change in the size of frazil that can be kept in suspension, at a critical fast ice thickness. Symbols and constants used are summarised in Table 1.

Table 1. Symbols and Constants

Symbol	value	units	definition
B		$\mathrm{m}^3.\mathrm{s}^{-3}$	buoyancy flux
C_d	1.3×10^{-3}		drag coeff
F	1 or 3/2		disc orientation factor
g	9.8	$\mathrm{m.s}^{-2}$	gravitational accn
h		m	sea ice thickness
r	0.004–5	mm	frazil disc radius
Re	$\frac{UL}{\nu}$		Reynolds number
S_i	5	psu	salinity of sea ice
S_w	35	psu	salinity in mixed layer
T_a	-25	°C	air temperature
T_f	-2	°C	freezing temperature
u_*	0.001–0.030	$\mathrm{m.s}^{-1}$	friction velocity
V		$\mathrm{m.s}^{-1}$	rise velocity
W_*		$\mathrm{m.s}^{-1}$	convective velocity scale
z_i	$25 - 75$	m	depth of mixed layer
ϵ	0.01		aspect ratio $t/(2r)$
κ	0.4		von Karman's constant
μ	1.88×10^{-3}	Pa.s	dynamic viscosity
ν	1.8×10^{-6}	$\mathrm{m}^2.\mathrm{s}^{-1}$	kinematic viscosity
ϱ_i	925	$\mathrm{kg.m}^{-3}$	density of sea ice
ϱ_w	1028	$\mathrm{kg.m}^{-3}$	density of seawater
ϱ_{ws}	0.81	$\mathrm{kg.m}^{-3}.\mathrm{psu}^{-1}$	$\frac{d\varrho_w}{dS}$

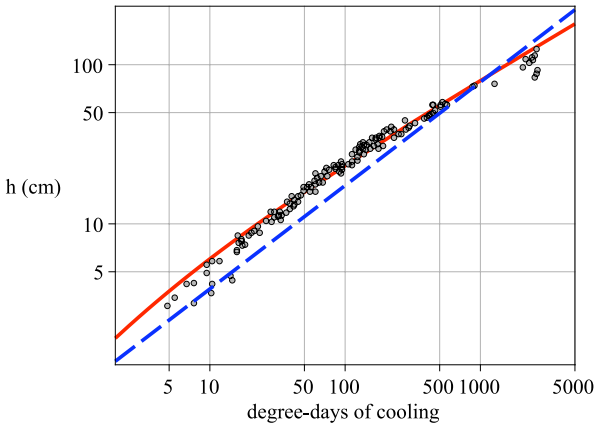

Figure 2. Data and a curve fitted by eye, for the thickness of snow-free ice versus the number of degree-days of cooling, taken near Greenland, after Anderson, 1961. Anderson's data is shown as filled circles, and his fit as a solid curve through them, on a log-log plot. Also shown is a dashed line, representing data from the shipping lane in McMurdo Sound, from the work of Purdie *et al*, 2006.

2. Brine Plume Velocities

We seek a representative velocity for brine plumes, to compare with the rise velocity of frazil crystals. The velocity of choice (McPhee and Morison, 2001) is the Deardorff (Deardorff, 1970) or free convection velocity scale W_*, which is a measure of the velocity expected to develop in an individual turbulent plume driven by a localised buoyancy source.

The Deardorff velocity may be written (e.g., McPhee and Morison, 2001)

$$W_*^3 = B\lambda \,, \tag{1}$$

where λ is a measure of the size of the dominant eddies, inferred from measurements (McPhee and Morison, 2001) to approach κz_i in the limit of negligible shear, where $\kappa = 0.4$ is von Kármán's constant. The term z_i is the thickness of the oceanic layer that is well-mixed by the rejected brine, that is, the depth to the pyncnocline, typically about 50 m in McMurdo Sound in mid-winter (Leonard *et al*, 2006), but reaching 75-100 m in the Weddell Sea. The simulations of Mellor *et al* (1986) also use a depth of 50 m for the well-mixed region. In general this depth will slowly grow, depending on the salinity versus depth curve that was in place in the seawater before the sea ice began to form, and the pycnocline at the bottom will be gradually eroded to greater depths. Since the mixed layer depth is a difficult concept in McMurdo Sound because of the weak stratification in the water column, and since mixing into the pyncnocline is a poorly understood problem (McPhee and Morison, 2001), we assume a constant $z_i = 50$ m here, but we later explore the sensitivity of our results to variations in z_i by also considering values of 25 and 75 m.

B is the buoyancy flux (Turner, 1979), here taken to be positive downwards,

$$B \equiv \frac{g\langle \varrho_w' w' \rangle}{\langle \varrho_w \rangle}$$

where $\langle \varrho_w' w' \rangle$ is the average downwards flux of random variations ϱ_w' in fluid density at the ice/water interface, and $\langle \varrho_w \rangle$ is the average density of seawater in the mixed layer.

A good fit to the dependence of the density of seawater on salinity S_w (psu) at the freezing point (Unesco, 1981) is

$$\varrho_w \approx 999.84 + \left(\frac{d\varrho_w}{dS}\right) S_w \,, \quad \text{where} \quad \frac{d\varrho_w}{dS} \equiv \varrho_{ws} \approx 0.81 \,,$$

so that

$$B \approx \frac{\varrho_{ws}\, g\langle w' S_w' \rangle}{\langle \varrho_w \rangle} \,. \tag{2}$$

The vertical flux of salt due to the freezing of the fast ice cover may be written in terms of its rate of growth $\dot{h}$ in the absence of frazil accretion, to get

$$\langle w' S_w' \rangle = \dot{h} \frac{\varrho_i}{\varrho_w} (S_w - S_i) \,, \tag{3}$$

where $\varrho_i \approx 925$ $\mathrm{kg.m}^{-3}$ is the density of the sea ice, and S_i is the salinity of the sea ice, typically proportional to the ocean salinity (Schmidt *et al*, 2004), so that $S_i \approx 0.14 S_w$. We approximate the density ϱ_w of brine immediately below growing sea ice by the density of the well-mixed layer (1028 $\mathrm{kg/m}^3$), and the salinity S_w by the salinity of the well-mixed layer, typically about 35 psu in McMurdo Sound.

Hence we have the convective velocity scale for brine plumes under growing sea ice W_*, given in terms of ice growth rate $\dot{h}$ by

$$W_*^3 = 0.344 g \varrho_{ws} \frac{\varrho_i}{\varrho_w^2} S_w z_i \dot{h} \,. \tag{4}$$

The associated Reynolds number is (with $z_i = 50$ m, and at an ice thickness of 1 m, when $\dot{h} \approx 0.1$ μm/s, so that $W_* \approx 5$ mm/s)

$$\mathrm{Re} = \frac{UL}{\nu} \approx \frac{5 \times 10^{-3} \times 50}{1.8 \times 10^{-6}} \approx 1.4 \times 10^5 \,.$$

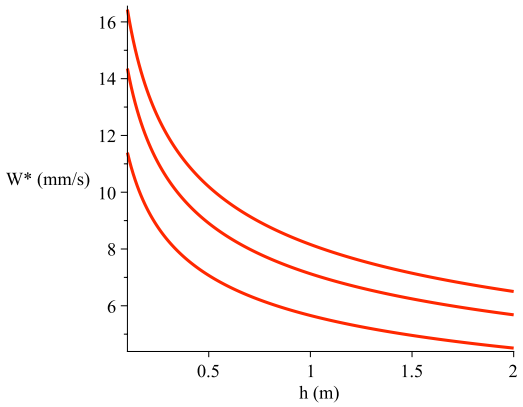

Figure 3. Calculated values of brine plume velocity versus sea ice thickness. There are three curves, the lower one is for $z_i = 25$ m, the middle one for $z_i = 50$ m and the upper one for $z_i = 75$ m.

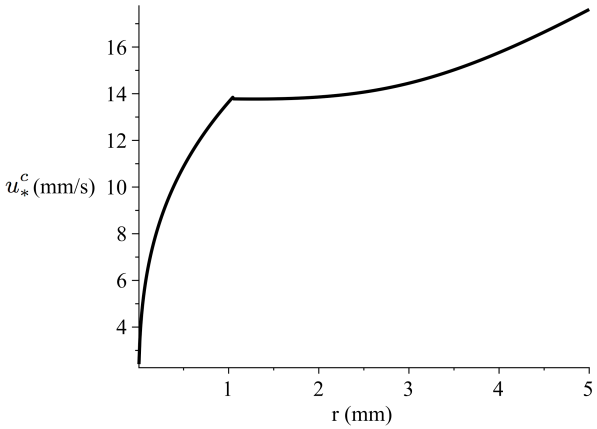

Figure 4. The Shields criterion for critical value of friction velocity (mm/s) against frazil disc radius (mm). When friction velocity takes the critical value, all frazil discs up to the indicated radius are mobilised by the turbulence.

This is consistent with turbulent plume flow, as it is much bigger than the critical value of about 200 for buoyant plumes (Snyder, 1981).

Niedrauer and Martin (1979) measure a brine flowrate of 0.25 mm/s, in an experiment with $z_i \approx 0.1$ m and $\dot{h} \approx 1 - 5$ μm/s. Then equation (4) gives $W_* \approx 2$ mm/s, which is a factor of eight higher than their observed brine flowrate. This is likely to be due to the effect of the plastic side-walls in their experiment, which are sufficiently close together to damp plume flows. With a spacing of just 1.6 mm between walls, the apparatus is essentially a Hele-Shaw cell, and plume flow is not turbulent. Indeed, a Reynolds number calculation gives

$$\mathrm{Re} = \frac{UL}{\nu} \approx \frac{0.25 \times 10^{-3} \times 1.6 \times 10^{-3}}{1.8 \times 10^{-6}} \approx 0.25 \ ,$$

which is much less than 200, so that plume flow is dominated by viscous effects at this Reynolds number.

Voropayev and Fernando (1999) grow sea ice in a box measuring 30x61 cm^2 in cross section and 60 cm in depth. They have a depth to pyncnocline of 0.2 m, and ice growth rates of 1–4 μm/s. Then our velocity scale predicts brine plume velocities $W_* \approx 2 - 3$ mm/s in their experiments, consistent with their calculations of brine plume velocities of 1–4 mm/s. The Reynolds number for their experiment is Re$\approx$ 400, just high enough to be turbulent.

3. Ice Growth Rate

We need ice growth rates to calculate brine rejection rates. Measurements of the thickness of snow-free ice (Anderson, 1961) in Thule, Greenland, provide direct estimates for growth rate as a function of ice thickness and air temperature. Anderson fitted the formula

$$h^2 + 0.051h = 0.775 \times 10^{-8} \ \theta \qquad (5)$$

where h is in m,

$$\theta \equiv \int_0^t (T_f - T_a) \ dt$$

is the number of degree-seconds of cooling, T_f is the temperature of the interface between ice and ocean (at freezing-point), and T_a is the air temperature, both in °C. This formula, which is derived from a simple model of sea ice growth (see also Lepparanta, 1993; Voropayev and Fernando, 1999), is illustrated together with Anderson's data in Fig. (2). It follows from Anderson's formula that

$$\dot{h} = \frac{0.775 \times 10^{-8}}{2h + 0.051}(T_f - T_a) \ . \qquad (6)$$

Measurements in McMurdo Sound (Leonard *et al*, 2006) give an eventually more rapid growth, as also illustrated in Fig. (2). This may be due to delayed accretion of frazil ice to the fast ice-ocean interface, leading to the incorporated platelet ice seen in cores. We use Anderson's data as a proxy for ice growth rate in the absence of frazil accretion, since frazil accretion does not in itself lead to brine rejection from the fast ice interface, and since incorporated platelets are not observed in fast ice cores from the Arctic.

Air temperatures of -25°C and a freezing temperature of -2°C will be used in Anderson's empirical formula, when illustrating typical growth rates. This leads to the values of W_* graphed against sea ice thickness in Fig. (3), for mixed layer depths of 25, 50 and 75 m.

4. Frazil Mobilisation Criteria

Two mechanisms for mobilising frazil are considered, a Shields criterion from sedimentation theory for turbulence to mobilize frazil, and brine plume velocity matching frazil rise velocity. The second mechanism varies with ice thickness, so has the possibility of explaining delayed emplacement of frazil in the ice cover, while the first does not, unless the only source of turbulence is the brine plumes. Both mechanisms interact with each other, since brine plumes contribute to the level of turbulence, and turbulence is known to modify the rise velocity of frazil.

4.1. Shields Criterion

Jenkins and Bombosch (1995) use a Shields criterion for deposition of frazil rising in a turbulent plume under an ice shelf. They note that their formulation is only appropriate for a grain Reynolds number greater than ∼1, corresponding to a frazil disc radius greater than ∼1 mm. Frazil sizes can be much smaller than this. Extensions to smaller grain Reynolds numbers have been made (Miller *et al*, 1977). Cao *et al* (2006) report an explicit relationship covering a wide

range of particle sizes, which we adopt. This relationship says that all frazil with radii less than or equal to r are mobilised when the friction velocity (u_*, a measure of the turbulent velocity scale) exceeds the critical value

$$u_*^c = \sqrt{2rg(1-\varrho_i/\varrho_w)\theta_c}\ ,$$

where the critical value of the Shields parameter has been carefully matched to experimental data to get

$$\theta_c = \begin{cases} 0.1414\mathrm{Re_g}^{-0.2306} & ,\ \mathrm{Re_g} < 6.61 \\ \dfrac{[1+(0.0223\mathrm{Re_g})^{2.8358}]^{0.3542}}{3.0946\mathrm{Re_g}^{0.6769}} & ,\ 6.61 \le \mathrm{Re_g} \le 282.84 \\ 0.045 & ,\ \mathrm{Re_g} > 282.84 \end{cases}$$

and $\mathrm{Re_g} = 2r\sqrt{2rg(1-\varrho_i/\varrho_w)}/\nu$ is the grain Reynolds number.

A graph of u_*^c versus r is shown in Fig. (4), with u_*^c taking values up to nearly 20 mm/s for the largest frazil sizes we expect. This may be compared with the range of values $u_* = 1 - 30$ mm.s^{-1} measured by McPhee *et al* (1999) in 1 m thick winter pack ice in the Weddell Sea. Typical values are 10–20 mm.s^{-1}. At the low end of this range, some larger frazil discs can settle against the solid ice cover. At values above 15 mm.s^{-1}, very little frazil in the size range of interest can settle out.

Brine plumes also contribute to friction velocity. But as we saw in Fig. (3), brine plume velocities are of the order of 5-15 mm.s^{-1}, giving an additive contribution of $\sqrt{C_d}\,W_* \approx$0.2–0.5 mm/s to the friction velocity (e.g., Beljaars, 1995; Grachev *et al*, 1998), where the drag coefficient $C_d \approx 1.3\times10^{-3}$ (e.g., Holland and Jenkins, 1999). So brine plumes may augment a shear-induced turbulent environment by only 1–2%, and in the absence of shear are too weak to mobilise any but the very smallest frazil through the Shields criterion, so we do not consider this further.

Brine plumes differ crucially from shear flow, in that they produce a net downflow, which rising frazil must conquer in order to settle out. So we now consider the rise velocity of frazil, in an environment where turbulence may take various values, from zero to those mentioned above.

4.2. Frazil Rise Velocity

Measurements of observed frazil rise velocities in fresh water (Gosink and Osterkamp, 1983) have been modelled by matching buoyancy and drag forces, where the drag force is given by a quadratic dependence on rise velocity, modified by a velocity-dependent coefficient of drag. Such a dependence allows the theory to cover both linear and nonlinear drag regimes, since the drag coefficient becomes inversely proportional to velocity in the low Reynolds number limit (Stokes flow limit), making the overall dependence linear in rise velocity. The frazil disc sizes they consider have radii in the range 0.5–3 mm, with Reynolds numbers from 1–75, and they note that Stokes' theory is not appropriate for the larger sizes (Re>5). However, their treatment of frazil disc orientation is very simple - they replace the disc with a sphere of the same radius, for the purposes of drag calculations.

The rise velocities of frazil observed by Gosink and Osterkamp (1983) and shown here in Fig. (5) lie in the range 5–15 mm.s^{-1}, which matches the range of brine plume velocities calculated in section (2). This already indicates, regardless of the model chosen for frazil rise velocity, that brine rejection is of the right order of magnitude to mobilise frazil rising in a non-turbulent (laminar) environment.

The very recent work of Morse and Richard (2009) is prompted by their study of acoustic measurements of frazil concentrations in a flowing river. They conduct an extensive and detailed review of frazil rise velocities, and they also consider work done on the terminal velocities of droplets and crystals falling through the atmosphere. Their preferred model is a power law fit by Khvorostyanov and Curry (2002) with continuously varying parameters over the size spectrum found in the atmosphere, which spans both Stokes and turbulent flow regimes, and is valid for Reynolds numbers up to 5000. Morse and Richard (2009) use data from the field and lab work of Gosink and Osterkamp (1983), and lab data from Wuebben (1984), to evaluate frazil rise models. They give a simple approximation (also valid for Re up to 5,000) to their preferred model for frazil discs which can be written as

,

$$W_r = \begin{cases} 6.229r^{1.621}\ , & r \le 0.635 \text{ mm} \\ -0.412r^2 + 8.138r - 2.024\ , & r > 0.635 \text{ mm} \end{cases} \quad (7)$$

where W_r is the rise velocity in mm.s^{-1} and r is disc radius in mm.

The rise velocity given by this approximation is graphed together with the data of Gosink and Osterkamp (1983) and Wuebben (1984), in Fig. (5). It is a good fit to the data. But the scatter of data allows a number of models.

For smaller frazil discs, with radii in the range 0.004–1 mm, it is appropriate to calculate the frazil rise velocity V using a Stokes flow analysis, since the Reynolds number $\mathrm{Re} = 2Vr/\nu$ is less than 1. An advantage of the Stokes flow analysis is that it allows us to compute explicitly the effect of disc orientation and aspect ratio, on rise velocity.

4.2.1. In Still Water

When discs move under the influence of their own buoyancy in a still viscous fluid, they exhibit a behaviour that ranges from steady movement with the surface normal aligned with gravity, through periodic motion to chaotic or tumbling motion (Field *et al*, 1997), depending on their size and relative density. For ice discs with radii up to 10 mm and an aspect ratio of 0.01 rising in still water, the steady behaviour is observed, with the largest surface area presenting at right angles to the flow (that is, with the c-axis vertical, as also observed in frazil experiments in salt water by Ushio and Wakatsuchi, 1993). Stokes flow at velocity V past a thin disc of radius r in this orientation (Lamb, 1932) leads to the viscous drag force

$$6\pi\mu RV \quad (8)$$

where $R = 8r/(3\pi)$, and $\mu \approx 1.88\times10^{-3}$ Pa.s is the dynamic viscosity of sea water. Matching this force with the buoyancy force $g(\varrho_w - \varrho_i)2\epsilon\pi r^3$ gives

$$V = \frac{\pi g(\varrho_w-\varrho_i)\epsilon r^2}{8\mu} \approx 2.1\times10^3\ r^2\ . \quad (9)$$

In the turbulent environment induced in the ocean by shear flow and plumes, it is to be anticipated that the above analysis for discs rising in still water should be modified. Two consequences are considered here, that the orientation of the disc is not necessarily with the c-axis vertical, and that turbulent vortices directly affect the rise velocity.

4.2.2. Disc Orientation In Turbulent Water

When a disc rises with the c-axis horizontal (that is, thin edge up), there is a different value $R = 16r/(9\pi)$ in the drag force given by expression (8) (Lamb, 1932). Since this is 3/2 times the R value for discs rising face-up, matching the drag force with buoyancy gives a rise velocity that is exactly half again as large as when discs rise face-up (9). So we will allow for the possibility that rise velocity is up to 50% larger,

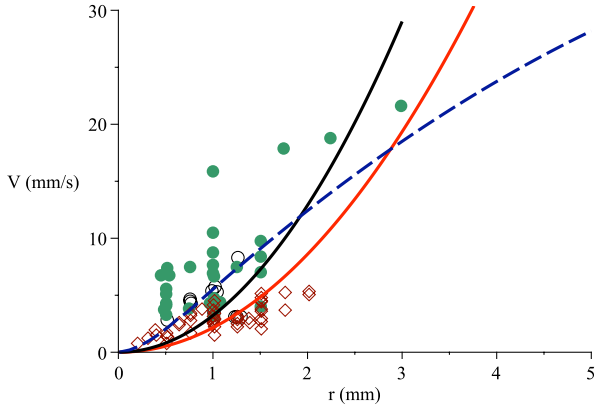

Figure 5. Frazil rise velocities V versus disc radius r, in still water. Filled discs are field observations by Gosink and Osterkamp (1983), circles are their lab data, and diamonds are lab data from Wuebben (1984). The dashed line is the Morse and Richard data fit given by equation (7). The solid lines are from a Stokes flow analysis, for a disc rising face up (the lower curve), and edge up (the upper curve), in still water.

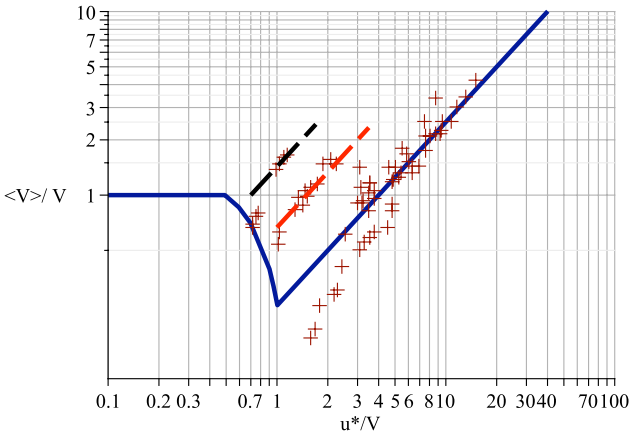

Figure 6. Observed mean diesel droplet rise velocities $\langle V \rangle$ versus friction velocity u_*, both normalised on the rise velocity V in still water, data from Friedman and Katz (2002) as crosses, and our hand-fitted behaviours shown as solid and dashed lines.

in our analysis, since discs in a turbulent environment may be at some time-varying angle between face-up and edge-up, and the actual velocity is expected to vary between these two values. We can write the rise velocity for both orientations in the form

$$V = \frac{\pi g(\varrho_w - \varrho_i) F \epsilon r^2}{8\mu} \,, \qquad (10)$$

where the disc orientation factor $F = 1$ for discs rising face-up, and $F = 3/2$ for discs rising edge-up (obtained directly from the ratio of the two different R values).

The effect of a 50% increased aspect ratio ϵ can also be seen from the effect of changing F, directly from Fig. (5), since aspect ratio simply multiplies F, the disc orientation factor, in equation (10).

The rise velocities predicted by this formula are compared in Fig. (5) with the velocities observed in experiments by Gosink and Osterkamp (1983) and Wuebben (1984), and with the formula (7) favoured by Morse and Richard (2009). The Stokes formulae sit at the lower end of data values when r is small, with for example rise velocity in the range 2.5–3.7 mm/s depending on disc orientation predicted when radius is 1 mm. At this radius, the Stokes analysis should be marginal since Reynolds number is just greater than two, but the match with data and with Morse and Richard's high Reynolds number fit is reassuring, especially for the face-up case. At disc radii greater than 3 mm, the Stokes theory begins to deviate from data and from the Morse and Richard model.

At smaller radii, the Reynolds number drops off rapidly (as the cube of r) — it is Re$\sim$0.3, for $r = 0.5$ mm, and the Stokes analysis is valid for $r \leq 0.5$ mm. However, at this radius most of the experimental data plots above the two Stokes curves in Fig. (5). This may be due to entrainment, where smaller discs are affected by the wake of bigger discs rising faster above them. Such entrainment effects, observed and noted in Gosink and Osterkamp (1983), suggest that the smaller velocities at each radius are more trustworthy, and may lead to bias in models like Morse and Richard's, which rely on a fit to all data. Such fitted models may over-estimate rise velocities for smaller discs.

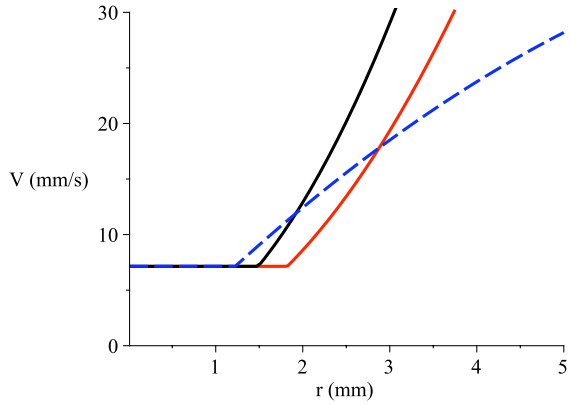

Figure 7. Modelled frazil rise velocity versus disc radius, modified by turbulence to level out at $u_*/0.7$, illustrated here for $u_* = 5$ mm/s, for Stokes theory with discs rising face-up (lower solid curve) and edge-up (upper solid curve), and for Morse and Richard's Case C (dashed line).

4.3. Turbulent Rise Velocities

Fluid turbulence can alter the settling velocity of solid particles, or the rise velocity of buoyant particles and bubbles, increasing or decreasing it, depending on the relative density of the particle and on the level of turbulence (Nielsen, 2007). This is because, for example, a heavy particle can spend more time in the upflow region of a vortex than in the downflow region, reducing its settling velocity. The closest analogue to frazil discs in that study is the movement of diesel drops in water, with a relative density of 0.85, which is experimental data originally from Friedman and Katz (2002). Nielsen notes that smaller drops of diesel are affected by turbulence in a similar manner to particles that are denser than water, spending more time in upflow regions of vortices, enhancing diesel rise velocities by this trajectory biassing. Hence we anticipate that the diesel results are a good indication of what to expect for the case of frazil, which is slightly heavier with a relative density about 0.9.

The experimental results of Friedman and Katz (2002) are graphed here in Fig. (6). They summarise their very detailed results by noting that:

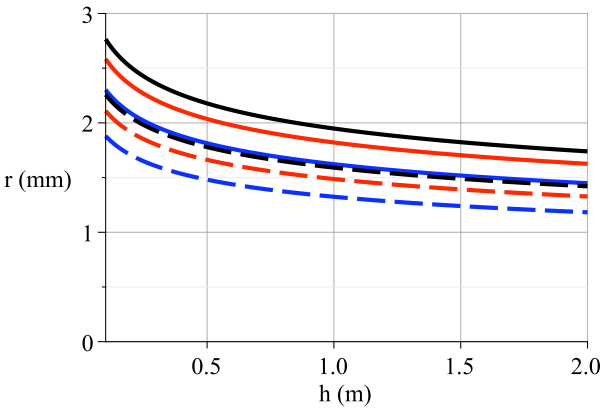

Figure 8. The maximum radius r (mm) of frazil discs that may be mobilised by brine rejection from fast ice of thickness h (m). Solid curves are for discs rising face-up, and dashed curves are for discs rising edge-up, in still water. The lower curve in each set (solid or dashed) uses a mixed layer thickness of 25 m, the middle curve 50 m, and the upper curve 75 m.

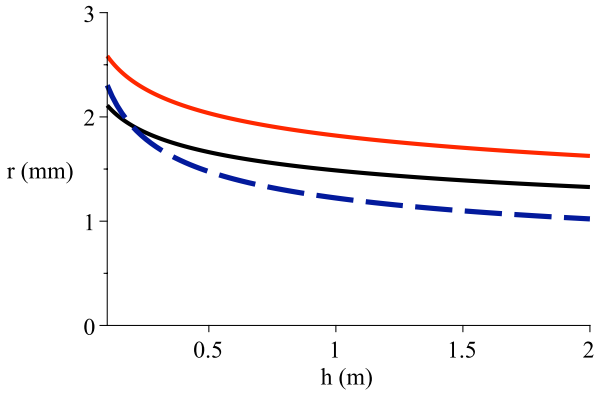

Figure 9. The maximum radius r (mm) of frazil discs that may be mobilised by brine rejection from fast ice of thickness h (m), using rise velocities in still water. A comparison of Stokes theory to Morse and Richard's (2009) Case C. The upper solid curve is for Stokes flow with discs rising face-up, the lower solid curve is for Stokes flow with discs rising edge-up, and the dashed curve is for Morse and Richard's Case C.

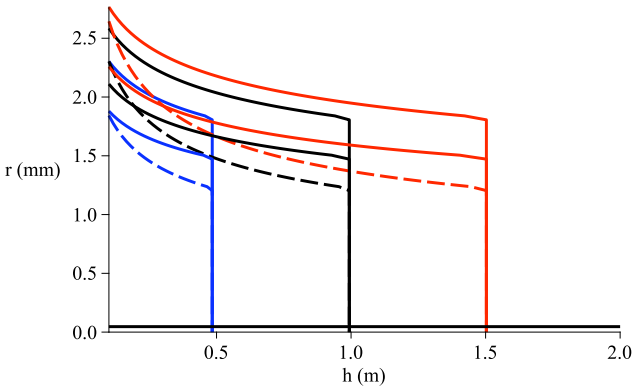

Figure 10. The maximum radius r (mm) of frazil discs that may be mobilised by brine rejection from fast ice of thickness h (m), in turbulent water. Friction velocity is 5 mm/s, and T_a is -25°C. The upper solid curve in each group of three is frazil rising face-up, the lower solid curve is frazil rising edge-up, and the dashed curve is Morse and Richard's Case C. The leftmost set of three curves, collapsing when turbulence dominates at $h \approx 0.5$ m, is for $z_i = 25$ m, the middle set which collapses at $h \approx 1$ m is for $z_i = 50$ m, and the rightmost set which collapses at $h \approx 1.5$ m is for $z_i = 75$ m. The solid horizontal line at $r = 0.05$ mm shows the Shields criterion — frazil smaller than this radius are mobilised by this level of turbulence.

1. At (relatively) high turbulence levels all droplets approach the speed $u_*/4$, with the exception of the two lowest turbulence levels.

2. At low turbulence levels all droplets are expected to approach the still water speed.

3. At intermediate turbulence levels, the results are mixed, depending on the relative inertia of droplets (the Stokes number).

The levels of turbulence in these experiments have root-mean-square fluctuation velocities that range from 30-180 mm/s, just above the range of friction velocities seen under pack ice (McPhee *et al*, 1999). The highest turbulence levels are the ones that approach the rise velocity $u_*/4$, illustrated by the solid straight line on the right-hand side in Fig. (6). The two lower turbulence levels, likely more relevant to our situation, level out at $u_*/1.5$ and $u_*/0.7$, as illustrated by the short dashed lines in that figure.

After studying both Fig. (6) and the figures in Friedman and Katz (2002) showing dependence of mean observed rise velocity $\langle V \rangle$ on droplet diameter, the rise velocity dependence on size may be summarised as:

1. Small droplets rise faster than in still water, approaching the speed $u_*/4$ for very large u_*, but approaching $u_*/0.7$ at the lowest turbulence levels, corresponding to the very highest levels of turbulence observed under pack ice.

2. Large droplets rise at the same rate as in still water.

What is interesting about smaller frazil having the same rise velocity, dependent on turbulence level rather than disc size, is that it raises the possibility of a sudden jump in the size of frazil that can settle out in a turbulent environment, that is, of a sudden collapse of mobilised frazil at a critical solid ice thickness. This sudden deposition of frazil is associated with the leveling out of the frazil rise velocity curve at a value related to turbulence levels.

We consider the consequence for frazil deposition of modified rise velocities, leveling out for small frazil sizes at a minimum value of rise velocity related to u_*. The actual value is rather uncertain, but we use the value $u_*/0.7$ to illustrate the effect of turbulence (Fig. (7)), as it is the behaviour in Friedman and Katz (2002) that is closest to our situation.

5. Critical Ice Thickness in Laminar Flow

Here we use the rise velocities of frazil in still water — this would strictly only apply in the case of a laminar plume downflow, but turns out to be relevant to larger sized discs in a turbulent environment, and is used here to highlight the effects of turbulence in following sections. Matching the brine plume velocity with the rise velocity of frazil of radius r and aspect ratio ϵ in still water gives (in the case of Stokes flow)

$$\frac{\pi g(\varrho_w - \varrho_i) F \epsilon r^2}{8\mu} = 0.0014 \left[\frac{g \varrho_{ws} \varrho_i S_w z_i (T_f - T_a)}{\varrho_w^2 (2h + 0.051)} \right]^{\frac{1}{3}},$$

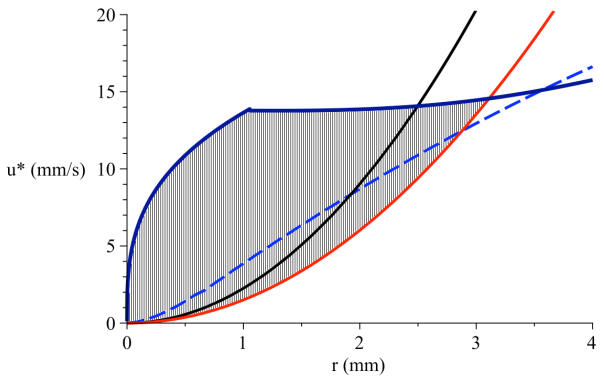

Figure 11. The Shields criterion for critical value of friction velocity (mm/s) against frazil disc radius (mm), shown on the same graph as the value of radius r where frazil rise velocity equals $u_*/0.7$. The dashed curve is for Morse and Richard's Case C, the lower solid curve is for Stokes theory for discs rising face-up, the solid curve immediately above it is for Stokes theory for discs rising edge-up.

so that critical thickness h of fast ice, at which all frazil of radius less than or equal to r is mobilised, satisfies the equation

$$r = \sqrt{\frac{0.0112\mu}{\pi g(\varrho_w - \varrho_i)F\epsilon}} \left[\frac{g\varrho_{ws}\varrho_i S_w z_i (T_f - T_a)}{\varrho_w^2(2h + 0.051)}\right]^{\frac{1}{6}} . \quad (11)$$

This relationship is graphed in Fig. (8) for discs rising face up and edge up. The graph illustrates that brine plume velocity is powerful enough to keep frazil sizes up to 2.5 mm in radii mobilised while ice thickness increases to 2 m. That is, smaller frazil sizes cannot settle out, in a non-turbulent environment, unless brine plume velocity is reduced, for example, if air temperature is much warmer than the -25°C used here for illustration.

Furthermore, in these laminar flow results, the radius r below which frazil is mobilised when sea ice reaches thickness h, does not vary much with h, due to the 1/6 power in the formula. When the sea ice reaches 1 m thick, and the mixed layer is 50 m thick, then frazil with radii greater that 1.7 mm rising face-up (or 1.4 mm rising edge-up) are able to settle against the fast ice, for example, and smaller frazil remain mobilised. Changing the mixed layer thickness to 25 m or 75 m changes the critical frazil size by up to 10%, as illustrated. We also looked at a 100 m thickness, and saw a 10% increase on the 50 m results. The formula (11) shows that exactly the same changes in h result from doubling or halving the thermal drive term $T_f - T_a$, or from doubling or halving S_w. Frazil rising edge-up rises faster, and is less readily mobilised, but this only makes a 20% difference in the size of frazil that is mobilised.

Since the Stokes flow assumption fails at larger frazil disc sizes, we also graph in Fig. (9) the relationship between frazil radius and ice thickness that is obtained if we use Morse and Richard's rise velocity (7) instead of the Stokes values, for the case that $z_i = 50$ m and $T_a = -25°$C. The figure shows that the higher rise velocities predicted by Morse and Richard's model for smaller frazil lead to a little more frazil ice settling out, but not much more than the Stokes flow predictions. At 1 m ice thickness, the Morse and Richard model has all frazil with radii less than 1.2 mm settling out, compared to 1.4 and 1.7 mm for the two Stokes cases.

6. Critical Ice Thickness in Turbulent Water

Now we illustrate the effect of a turbulence-induced cutoff in rise velocity on frazil mobilisation. We use $u_* = 5$ mm/s for illustration. Using the modified rise velocity curves illustrated in Fig. (7) to match brine plume velocity leads to the frazil deposition curves in Fig. (10). They are modifications of the curves in Fig. (8) for the laminar case.

The remarkable feature of these modified curves is the sudden deposition of most frazil sizes present, when solid ice thickness reaches the critical value corresponding to the switch of rise velocity to $u_*/0.7$. All frazil with this rise velocity is abruptly able to settle out, down to the frazil sizes mobilised by the Shields criterion, indicated by the horizontal line near the the $r = 0$ axis in Fig. (10).

The other matter to consider when we allow for a rise velocity modified by turbulence, is whether this level of turbulence will mobilise frazil in any case, according to the Shields criterion. For example, when $u_* = 5$ mm/s, the Shields criterion says that frazil smaller than about 0.05 mm in radius will be mobilised. This should be compared to the radius at which the switch to a constant rise velocity occurs in Fig. (7), approximately 1–2 mm. If u_* is larger than 15 mm/s, Fig. (4) indicates that all frazil with disc radius less than 4 mm is mobilised by the Shields criterion.

It is instructive to show the Shields criterion on the same graph as the frazil radius at which the catastrophic jump in rise velocity occurs, as in Fig. (11). The region between the Shields curve and the Stokes face-up curve is shaded in this figure. A horizontal line at a given value of u_* in the shaded region, will start at a minimum r value and end at a maximum r value, giving the range of frazil radii that are suddenly deposited when the critical ice thickness is reached where brine plume velocity matches $u_*/0.7$, using the Stokes face-up model.

The size of this sudden jump in frazil size deposited is largest when u_* is in the range 3–13 mm/s, values seen in McPhee *et al* (1999). As u_* decreases, the jump size reduces and the jump is delayed to thicker sea ice and smaller frazil radii.

7. Conclusions

Our results indicate that as the solid sea ice cover thickens, brine rejection slows and allows smaller and smaller frazil to settle against and freeze onto the interface. Ice cover thickness is typically of the order of 1 m for frazil of radius 1-2 mm to begin to stick to the ice cover, indicating that brine rejection is powerful enough to keep a significant size range of frazil in suspension if turbulence is ignored.

Our models predict only a gradual change in the maximum size of frazil that can settle out, as ice thickness changes from 0.1 to 2 m, unless the effects of turbulence are included. Turbulence can significantly alter the frazil rise velocity curve, leading to the sudden deposition of a range of frazil sizes when conditions are right. Our calculations were for the particular case that friction velocity is 5 mm/s, but serve to illustrate the observation that frazil rise velocities are expected to be almost independent of size over a range of (smaller) frazil sizes in a turbulent environment, and that this may lead directly to a sudden transition from mobilised to settled frazil, as brine plume velocities decrease. The range of frazil sizes that experience a constant rise velocity depends on turbulence levels, and is typically all discs up to about 2 mm in radius.

We have considered the effects of brine plumes on a single frazil disc. But when a number of frazil discs accumulate, they will in turn modify the flow environment. In particular, an important mechanism that is outside the scope of

this study is the stabilising effect that accumulating buoyant frazil may have on turbulence, by altering the density gradient of the mixture of seawater and frazil ice, and by increasing its viscosity.

Once enough frazil has been produced, turbulent stirring (due to both shear flow and brine rejection) near the ice-ocean interface might be stabilised sufficiently that frazil can settle against the interface, as is known to be possible with stratified cohesive sediments (Winterwerp, 2001), which can collapse in a positive feedback process. To study this would require a model of frazil growth and generation in the well-mixed ocean layer, coupled with a model of fast ice growth, and with a model for the vertical distribution of frazil ice in a turbulent buoyant environment. Both congelation ice growth from the fast ice layer, and frazil ice growth in suspension below, would then compete to relieve supercooling in such a model.

There remains a broad question about the role and modelling of platelet ice in the growth of first-year sea ice in Antarctica. It can occupy one-third to one-half of the total landfast sea ice thickness near ice shelves. Platelet ice is clearly an important component of Antarctic sea ice, but it is not yet accounted for in sea ice growth models and remains poorly understood.

Acknowledgments. The authors would like to thank the Marsden Fund of New Zealand, the University of Otago in New Zealand, the Korea Advanced Institute of Science and Technology in South Korea, and Victoria University of Wellington in New Zealand, for the support that enabled this work to proceed.

References

Anderson, D.L. (1961) Growth rate of sea ice, *J. Glaciol. 3* 1170–1172.

Bombosch, A. (1998) Interactions between floating ice platelets and ocean water in the southern Weddell Sea, *AGU Antarct. Res. Ser.* (Ocean, ice, and atmosphere: Interactions at the Antarctic continental margin, ed. by S.S. Jacobs), *75*, 257-266. Interactions between floating platelets .... in Ocean, Ice Atmosphere: *Antarctic Research Series 75* AGU, 257–266.

Badillo, A., and C. Beckermann (2006) Phase-field simulation of the columnar-to-equiaxed transition in alloy solidification, *Acta Materialia 54* 2015–2026.

Beljaars, A.C.M. (1995) The parameterization of surface fluxes in large-scale models under free convection, *Quart. J. Roy. Met. Soc. 121* 255–270.

Cao, Z., G. Pender, and J. Meng (2006) Explicit formulation of the Shields diagram for incipient motion of sediment, *Jour. Hydraulic Eng. 132* 1097–1099. DOI:10.1061/ASCE0733-94292006132:101097

Crocker, G.B., and P. Wadhams (1989) Modelling Antarctic fast-ice growth, *Journal of Glaciology 35* (119) 3–8.

Daly, S.F. (1984) *Frazil Ice Dynamics*, CRREL Monograph *84-1*, USA Cold Regions Research and Engineering Laboratory, Hanover NH.

Deardorff, J.W. (1970) Convective Velocity and Temperature Scales for the Unstable Planetary Boundary Layer and for Rayleigh Convection, *J. Atmos. Sci. 27* 1211–1213.

Dieckmann G., G. Rohardt, H. Hellmer, and J. Kipfstuhl (1986) The occurrence of ice platelets at 250 m depth near the Filchner Ice Shelf and its significance for sea ice biology. *Deep-Sea Res 33:* 141–148.

Eicken, H. (2003) From the microscopic, to the macroscopic, to the regional scale: Growth, microstructure and properties of sea ice, Chapter 2 in *Sea Ice — An introduction to its physics, chemistry, biology and geology*, Editors Thomas, D.N., and Dieckmann, G.D., Blackwell Publishing, Oxford, UK.

Field, S.B., M. Klaus, M.G. Moore, and F. Nori (1997) Chaotic dynamics of falling discs, *Letters to Nature 388* 252–255.

Friedman, P.D., and J. Katz (2002) Mean rise rate of droplets in isotropic turbulence, *Phys. Fluids 14* 3059–3073.

Ghosh, A. (2001) Segregation in cast products, *Sadhana 26*, Parts 1 and 2, 5–24.

Goring, D.G., and A. Pyne (2003) Observations of sea-level variability in Ross Sea, Antarctica, *NZ journal of marine and freshwater research 37* 241–249.

Gosink, J.P., and T.E. Osterkamp (1983) Measurements and analyses of velocity profiles and frazil-ice crystal rise velocities during periods of frazil ice formation in rivers, *Annals of Glaciology 4* 79–84.

Gow, A.J., S.F. Ackley, and J.W. Govoni (1998), Physical and structural properties of land- fast sea ice in McMurdo Sound, Antarctica, *Antarctic Research Series 74* 355–374.

Grachev, A.A., C.W. Fairall, and S.E. Larsen (1998) On the determination of the neutral drag coefficient in the convective boundary layer, *Boundary Layer Meteorol. 86* 257–278.

Holland, P.R., and D.L. Feltham (2005) Frazil dynamics and precipitation in a water column with depth-dependent supercooling. *J. Fluid Mech. 530* 101–124.

Holland, D.M., and J.A. Jenkins (1999), Modelling thermodynamic ice-ocean interactions at the base of an ice shelf, *J. Phys. Oceanogr. 29* 1787–1800.

Jeffries, M.O., W.F. Weeks, R. Shaw, and K. Morris (1993) Structural characteristics of congelation and platelet ice and their role in the development of Antarctic land-fast sea ice, *Journal of Glaciology 39*(132) 223–238.

Jenkins, A., and A. Bombosch (1995) Modeling the effects of frazil ice crystals on the dynamics and thermodynamics of Ice Shelf Water plumes, *J. Geophys. Res. 100*(C4) 6967–6981.

Jones, S.J., and B. Hill (2001) Structure of sea ice in McMurdo Sound, Antarctica, *Annals of Glaciology 33* 5–12.

Khvorostyanov, V.I., and J.A. Curry (2002) Terminal velocities of droplets and crystals: power laws with continuous parameters over the size spectrum, *Jour. Atmos. Sci. 59* 1872–1884.

Lake, R.A., and E.L. Lewis (1970) Salt rejection by sea ice during growth, *J. Geophys. Res. 75* No.3 583–598.

Lamb, Sir H. (1932) *Hydrodynamics*, Dover, NY.

Leonard, G.H., C.R. Purdie, P.J. Langhorne, T.G. Haskell, M.J.M. Williams, and R.D. Frew (2006) Observations of platelet ice growth and oceanographic conditions during the winter of 2003 in McMurdo Sound, Antarctica, *J. Geophys. Res. 111* (C04012), doi:10.1029/2005JC002952.

Lepparanta, M. (1993) A review of analytical models of sea-ice growth, *Atmosphere-Ocean 31* (1) 123–138.

MacAyeal, D.R. (1984) Thermohaline circulation below the Ross Ice Shelf: A consequence of tidally induced vertical mixing and basal melting, *J. Geophys. Res. 89* (C1) 597–606.

McPhee, M.G., C. Kottmeier, and J.H. Morison (1999) Ocean Heat Flux in the Central Weddell Sea during Winter, *Jour. Phys. Oceanography 29* 1166–1179.

McPhee, M.G., and J.H. Morison (2001) Under-Ice Boundary Layer, in *Encyclopedia of Ocean Sciences*, Academic Press, London, 3071–3078. doi:10.1006/rwos.2001.0146

Martin, S. (1981) Frazil ice in rivers and oceans, *Ann. Rev. Fluid Mech. 13* 379–397.

Miller, M. C., I.N. McCave, and P.D. Komar (1977) Threshold of sediment motion under unidirectional currents, *Sedimentology 24* 507–527.

Mellor, G.L., M.G. McPhee, and M. Steele (1986) Ice-seawater turbulent boundary layer interaction with melting or freezing, *J. Phys. Oceanogr. 16* 1829–1846.

Moretskii, V.N. (1965) Underwater sea ice, *Problemy Arktiki i Antarktiki 19:* 32–38. (Translation by E.R. Hope, DRB Canada Report No. T497R April 1968).

Morse, B., and M. Richard (2009) A field study of suspended frazil ice particles, *Cold Regions Sci. and Tech. 55* 86–102.

Niedrauer, T.M., and S. Martin (1979) An experimental study of brine drainage and convection in young sea ice, *Jour. Geophys. Res. 84*(C3) 1176–1186.

Nielsen, P. (2007) Mean and variance of the velocity of solid particles in turbulence, in *Particle Laden Flow: From Geophysical to Kolmogorov Scales*, editors B.J. Guerts, H. Clercx, and W. Uijttewaal, Springer, Netherlands, 385–391.

Purdie, C., P.J. Langhorne, G. Leonard, and T. Haskell (2006) Growth of first year land-fast Antarctic sea ice determined from winter temperature measurements. *Annals of Glaciology 44* Number 1, 170–176. doi:10.3189/172756406781811853

Schmidt, G.A., C.A. Bitz, U. Mikolajewicz, and L. Tremblay (2004) Ice-ocean boundary conditions for coupled models, *Ocean Modelling 7* 59–74.

Smedsrud L.H. (2001) Frazil ice entrainment of sediment: large tank laboratory experiments, *Journal of Glaciology Vol. 47* 461–471.

Smedsrud, L.H., and A. Jenkins (2004) Frazil ice formation in an ice shelf water plume, *J. Geophys. Res. 109* C03025 (15 pages). DOI: 10.1029/2003JC001851.

Smith, I.J. (2001) Platelet ice in McMurdo Sound, Antarctica, PhD thesis, Physics Department, University of Otago, New Zealand.

Smith, I.J., P.J. Langhorne, H.J. Trodahl, T.G. Haskell, R. Frew, and R. Vennell (2001) Platelet ice and the land-fast sea ice of McMurdo Sound, Antarctica, *Annals of Glaciology 33* 21–27.

Smith, I.J., P.J. Langhorne, H.J. Trodahl, T.G. Haskell, and D.M. Cole (1999) *Platelet ice - the McMurdo Sound Debate*, in H.T. Shen, ed., *Ice in Surface Waters - Proceedings of the 14th IAHR Symposium on Ice*, A.A. Balkema, Rotterdam, Netherlands, pp. 371–378.

Snyder, W. H. (1981) Guideline for fluid modelling of atmospheric diffusion, *US Environment Protection Agency Report No. EPA-600/8-81-009*, Research Triangle Park, N.C., U.S.A. (200 pages).

Svensson, U., and A. Omstedt (1994) Simulation of supercooling and size distribution in frazil ice dynamics, *Cold Regions Sci. and Tech. 22* 221–223.

Svensson, U., and A. Omstedt (1998) Numerical simulation of frazil ice dynamics in the upper layer of the ocean, *Cold Regions Science and Technology, 28* 29–44.

Turner, J.S. (1973) *Buoyancy Effects in Fluids*, Cambridge University Press.

Unesco (1981)— *Background paper and supporting data on the International Equation of State of Seawater*, Unesco Technical Papers in Marine Science 38, Unesco, Paris, France.

Ushio, S., and M. Wakatsuchi (1993) A laboratory study on supercooling and frazil ice production processes in winter coastal polynyas *J. Geophys. Res. 98*(C11) 20321–20328.

Veazey, A.D. (1994) Development and variability of the structure and physical properties of landfast sea ice in McMurdo Sound, Antarctica, Master's thesis, University of Alaska, Fairbanks, AK, USA.

Veazey, A.D., M.O. Jeffries, and K. Morris (1994) Small-scale variability of physical properties and structural characteristics of Antarctic fast ice, *Annals of Glaciology 20* 61–66.

Voropayev, S.I., and H.J.S. Fernando (1999) Evolution of two-layer thermohaline systems under surface cooling, *J. Fluid Mech. 380* 117–140.

Weeks, W.F., and S.F. Ackley (1986) The growth, structure, and properties of sea ice, in *The Geophysics of Sea Ice, NATO ASI Series, Series B: Physics, 146,* edited by N. Untersteiner, pp. 9–164, Plenum Press, New York, NY, USA.

Winterwerp, J.C. (2001) Stratification effects by cohesive and noncohesive sediment, *Jour. Geophys. Res., 106* No. C10, 22,559–22,574.

Wuebben, J.L. (1984) The rise pattern and velocity of frazil ice, in *the Proceedings of the Third Workshop on the Hydraulics of Ice Covered Rivers*, *Session F*, pp. 297–316, Committee on River Ice Processes and the Environment, Fredericton, Canada (www.cripe.ca).

M.J. McGuinness, Department of Mathematical Sciences, Korea Advanced Institute of Science and Technology, Taejon, South Korea. (Mark.McGuinness@vuw.ac.nz)

M.J.M. Williams, National Institute of Water and Atmospheric Research Ltd., Wellington, New Zealand. (m.williams@niwa.co.nz)

P.J. Langhorne, Physics Department, University of Otago, Dunedin, New Zealand. (pjl@physics.otago.ac.nz)

C. Purdie, Physics Department, University of Otago, Dunedin, New Zealand. (craigp@physics.otago.ac.nz)

J. Crook, School of Mathematics, Statistics and Operations Research, Victoria University of Wellington, New Zealand. (calljohno1@yahoo.com)